Applied Catalysis B: Environmental 168-169 (2015) 483–489

Contents lists available at ScienceDirect

Applied Catalysis B: Environmental

journal homepage: www.elsevier.com/locate/apcatb

A wide-spectrum-responsive TiO_2 photoanode for photoelectrochemical cells

Zhuofeng Hu [a], Jimmy C. Yu [a,*], Tian Ming [b], Jianfang Wang [b]

[a] Department of Chemistry, Shenzhen Research Institute and Institute of Environment, Energy and Sustainability, The Chinese University of Hong Kong, Shatin, New Territories, Hong Kong, China
[b] Department of Physics, The Chinese University of Hong Kong, Shatin, New Territories, Hong Kong, China

ARTICLE INFO

Article history:
Received 11 December 2014
Received in revised form 12 January 2015
Accepted 14 January 2015
Available online 15 January 2015

Keywords:
TiO_2 nanorod
Photoelectrochemical cell
Nitrogen-doped
Wide spectrum

ABSTRACT

A wide-spectrum-responsive photoanode was prepared by coating a 2–5 nm nitrogen-doped carbon (N—C) layer onto TiO_2 nanorod array in a solution of glucose and ethanediamine under hydrothermal condition. The nitrogen-doped carbon layer extended the photoresponse of TiO_2 nanorod array from UV to NIR region. Besides, the photocurrent of N—C—TiO_2 nanorod array was superior to that of pristine TiO_2 nanorod arrays with an on-set potential shifted negatively by 0.1 V. The N—C layer was found to behave like a p-type semiconductor and formed a *p–n* junction with the n-type TiO_2 nanorods. The N—C layer facilitated charge transportation and contributed to the generation of photocurrent under Vis and NIR illumination.

1. Introduction

Photoelectrochemical cells (PECs) are often used in converting solar energy to electrical energy and reducing carbon dioxide to clean fuels [1,2]. Titanium dioxide is the most widely studied material for photoanodes due to its high efficiency, low cost and environmental-friendliness [3]. However, with a bandgap of 3.2 eV, the anatase TiO_2 photoanodes requires UV excitation. This is a serious limitation for solar applications.

Much progress has been made to extend the response of TiO_2 to the visible light region (Vis). This can be achieved by doping [4–6] or building heterostructure [7,8]. However, the progress in the utilization of near infrared (NIR) light is much slower. To the best of our knowledge, the only method is to decorate sulfide semiconductors and up-conversion materials (such as $NaYF_4$:Yb^{3+} or carbon quantum dots) together on the TiO_2 photoanodes [9–11]. Under NIR light illumination, the visible light generated from the up-conversion materials excites the electron/hole pair in the sulfide semiconductors. Then, the electron/hole pair will be separated at the TiO_2/sulfide interface to form photocurrent. This method has three problems. First, the efficiency of the PECs would be limited due to multi-transfer of energy (from NIR to Vis then to electricity). Second, a sacrificial agent is needed to protect sulfide from photocorrosion [11]. Finally, it is not easy to maintain a strong binding between the additional materials and the TiO_2 substrate.

Carbon is known to resist photocorrsosion and it connects to metal oxide easily [12,13]. Its photoelectric property and bandgap can be adjusted by controlling the structure or doping hetero atoms [14–16]. Herein, a nitrogen-doped carbonaceous layer (N—C layer) is coated on the surface of TiO_2 nanorod as a new photoanode. For this composite material, photoresponse is observed in the NIR, Vis as well as UV light regions. photoexcited electron/hole pairs are produced directly in the N—C layer, and are separated efficiently at the interface between TiO_2 and the N—C layer.

2. Experimental

2.1. Preparation of TiO_2 nanorods on FTO glasses (TiO_2 NRs)

The TiO_2 nanorods array was grown on the surface of a Fluorine doped Tin Oxide (FTO) glass according to a procedure previously reported [17]. Briefly, 10 ml of concentrated hydrochloric acid was diluted with 10 ml deionized (DI) water, and 0.2 ml titanium isopropoxide were mixed in a 20 ml beaker. This clear solution was transferred to a Teflon-lined stainless steel autoclave (25 ml volume). Then, a clean FTO glass substrate was submerged in the solution. The sealed autoclave was heated in an electric oven at 150 °C for 5 h, and then cooled down to room temperature slowly. A white TiO_2 nanorod film was uniformly coated on the FTO glass substrate. The sample was thoroughly washed with DI water and

* Corresponding author. Tel.: +852 39436268.
E-mail address: jimyu@cuhk.edu.hk (J.C. Yu).

http://dx.doi.org/10.1016/j.apcatb.2015.01.018
0926-3373/

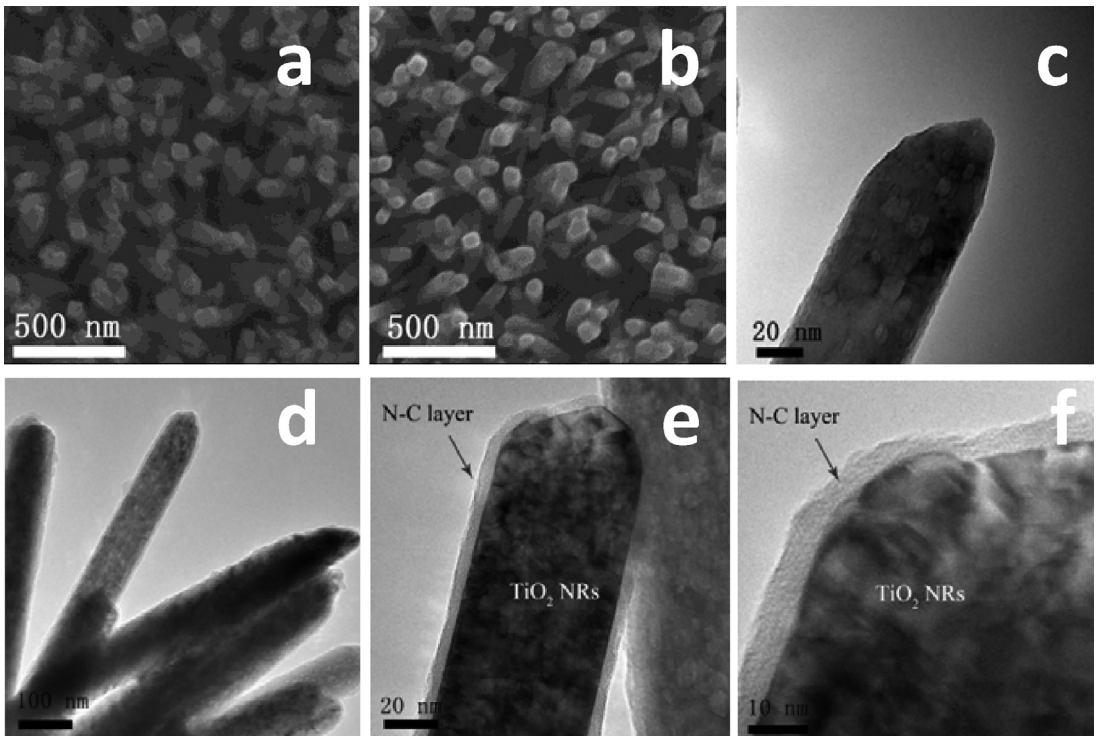

Fig. 1. SEM images of (a) TiO_2 NRs and (b) N—C—TiO_2 NRs; TEM images of (c) TiO_2 NRs and (e–f) N—C—TiO_2 NRs.

air dried. Finally, the sample was annealed in air at 550 °C for 3 h to increase the crystallinity of TiO_2 nanorods and improve their contact to the substrate.

2.2. Coating of nitrogen-doped carbonaceous layer on TiO_2 NRs

1 g of glucose and 0.1 mL of ethanediamine were dissolved into 20 mL of distilled water to form a homogeneous solution. Subsequently, the solution was transferred to a 25 mL Teflon-lined stainless steel autoclave. The TiO_2 NRs immersed into the solution, and heated at 180 °C for 4 h. After the reaction, the plate was taken out and washed with distilled water and ethanol before dried in a vacuum oven. For comparison, 0.1, 0.5, 2.0 and 4.0 g of glucose or 0.05 and 0.5 mL of ethanediamine were used to prepared different samples.

2.3. Characterization

Morphology of the products was characterized by scanning electron microscopy (SEM) on a FEI Quanta 400 microscope and by transmission electron microscopy (TEM) on a CM-120 microscope (Philips, 120 kV) coupled with an energy-dispersive X-ray (EDS) spectrometer (Oxford Instrument). X-ray diffraction (XRD) was performed on a Rigaku SmartLab X-ray diffractometer using a Cu Kα source irradiation (λ = 1.5406 Å). X-Ray photoelectron spectroscopy (XPS) was performed using a Sengyang SKL-12 spectrometer equipped with a VG CLAM 4 MCD electron energy analyzer and twin anode Mg Kα radiation (1253.6 eV) or Al Kα radiation (1496.3 eV) X-ray sources.

2.4. Photoelectrochemical measurements

N—C—TiO_2 NRs or N—C—TiO_2 NWs were fabricated into photoanode by securing a copper wire onto a bare portion the substrates via silver paste. All the photoelectrochemical measurements were performed in a thermostat-controlled standard three-electrode cell with a saturated-potassium–chloride silver chloride electrode (Ag/AgCl) as a reference electrode, a platinum foil ($1.0 \times 1.0\ cm^{-2}$) as a counter electrode, and a N—C—TiO_2 NRs or N—C—TiO_2 NWs as a working electrode. The electrolyte was 0.1 M Na_2SO_4. Linear sweeps and transient photocurrent were measured by a CHI 660D electrochemical workstation. A 980 nm near Infrared light laser and a 300 W Xenon arc lamp coupled with a AM 1.5G global filter ($100\ mW\ cm^{-2}$) were used as radiation source. The AM 1.5 global filter is an Air Mass Filter that corrects the output of a Xenon lamp to better match the solar spectrum for a 37 degree tilted surface from the ground. A UV cut-off filter and UV–vis cut off filter were used to simulate the Vis light and IR light.

2.5. Gas evolution measurements

The hydrogen and oxygen evolution by photoelectrochemical water splitting was conducted in the airtight H-type reactor connected to a closed gas circulation system (Fig. S5). A 300 W Xenon arc lamp coupled with a AM 1.5G global filter ($100\ mW\ cm^{-2}$) were used as radiation source. The amount of hydrogen and oxygen was measured by a gas chromatography equipped with TCD.

3. Results and discussion

3.1. Morphology and structure

TiO_2 nanorod arrays (TiO_2 NRs) were synthesized on a FTO glass according to the literature [17]. After reaction, a white homogeneous film of vertically aligned nanorods was observed on the FTO substrate, as shown in Fig. 1a. The nanorods with a rectangular cross section exhibit a diameter of about 100 nm.

Carbonaceous materials are formed via the cross-linking and intermolecular dehydration of glucose molecules under hydrothermal condition [18–20]. With the addition of N-containing precursors, nitrogen-doped carbonaceous material (N—C) with different electrical properties can be achieved. In our experiments,

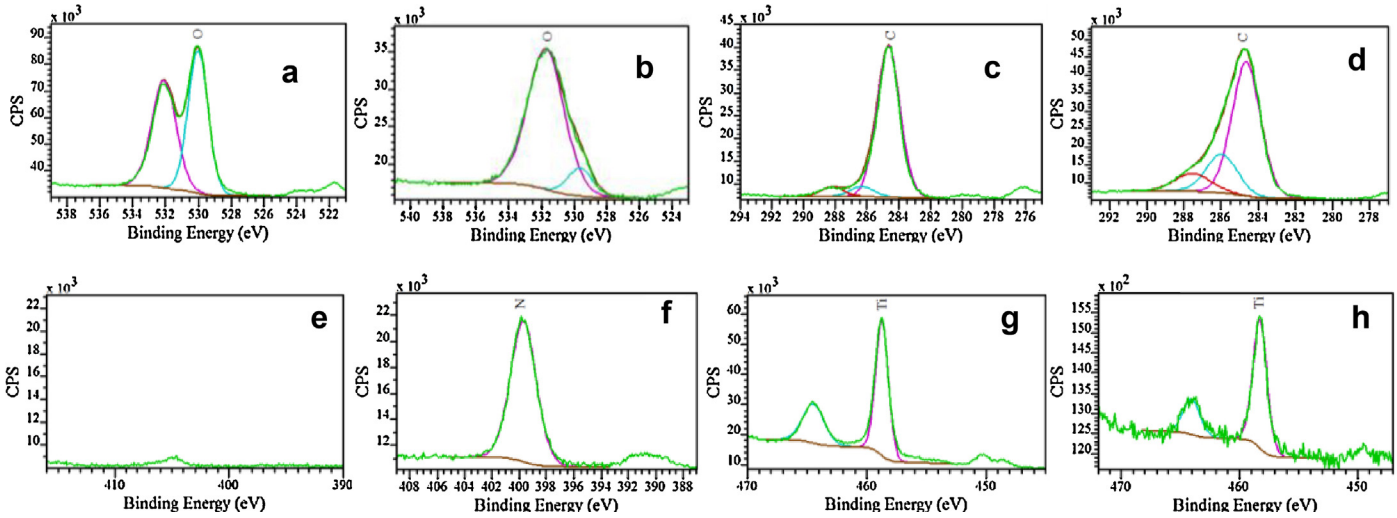

Fig. 2. O 1s XPS spectra of the (a) TiO_2 NRs and (b) N—C TiO_2 NRs; C 1s XPS spectra of the (c) TiO_2 NRs and (d) N—C TiO_2 NRs; N 1s XPS spectra of the (e) TiO_2 NRs and (f) N—C TiO_2 NRs; Ti 2P XPS spectra of the (g) TiO_2 NRs and (h) N—C TiO_2 NRs.

a layer of N—C was coated on the surface of TiO_2 nanorods array hydrothermally in a mixture solution of glucose and ethanediamine. The process is shown in Scheme 1.

The structure of nanorod remains after the hydrothermal reaction (Fig. 1b). A 3–7 nm amorphous N—C layer covers uniformly and intimately on the surface of TiO_2 NRs, as is shown in Fig. 1d–f. The TiO_2 NRs is confirmed as rutile by its XRD patterns (Fig. S1). With the N—C layer coated, the diffraction peaks related to TiO_2 NRs become weaker due to the blocking effect of the N—C layer. The N—C layer is confirmed to be amorphous by its XRD patterns due to the absence of diffraction peaks (Fig. S1).

Chemical states of the N—C TiO_2 NRs were investigated by XPS. The fine O 1s spectra of the TiO_2 NRs (Fig. 2a) can be deconvoluted into two peaks centered at 530.1 (lattice oxygen in TiO_2) and 531.9 eV (Ti—O—H at the surface or hydroxyl groups on the surface of TiO_2) [17,21,22]. The hydroxyl groups may be introduced during the preparation under hydrothermal condition. After the coating of the N—C layer, the peak at 531.9 eV increases noticeably compared with the peak at 530.1 eV, suggesting more hydroxyl groups are formed on the N—C TiO_2 NRs. In addition, a peak related to carboxyl group can be observed at 287.4 eV in the fine C 1s XPS spectra; and a N peak at 399.7 eV in the fine N 1s XPS spectra correspond to the pyrrole-like N [23].

The Ti 2p XPS spectra of TiO_2 NRs is deconvoluted into two peaks at 464.5 and 458.7 eV, which is in agreement with the values for typical TiO_2 [17,21,24]. After the coating the N—C layer, the Ti 2p spectra show similar peaks centered at 464.1 and 458.3 eV. This indicates that the structure of the TiO_2 NRs does not change after N—C coating.

3.2. Photoelectrochemical measurements

PEC measurements were conducted in a three-electrode electrochemical cell in 0.1 M Na_2SO_4 solution. The Linear sweep voltammograms were recorded under the radiation of a 1 W cm^{-2} 980 nm near infrared light laser in the potential range of −0.4 to 0.4 V vs. Ag/AgCl, as shown in Fig. 3a. The radiation was chopped every 4 s.

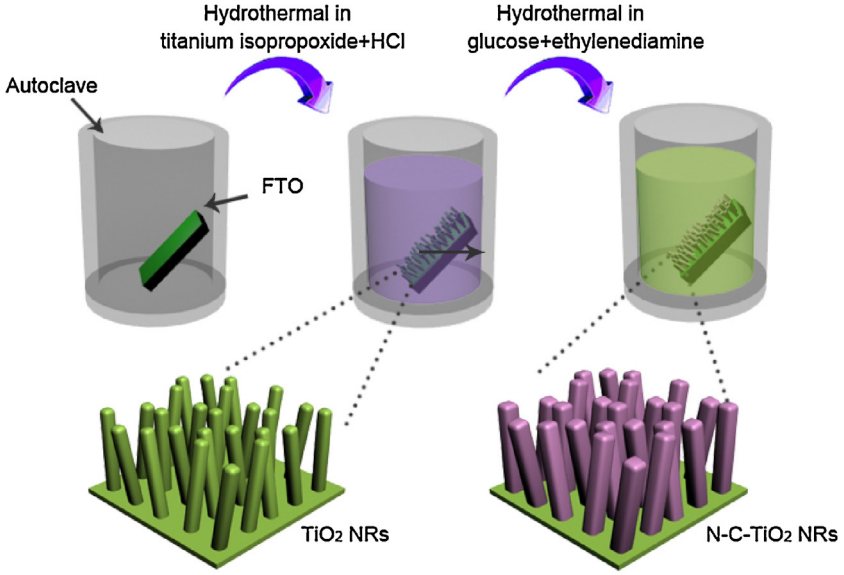

Scheme 1. Schematic diagram showing the preparation of N—C—TiO_2 NRs.

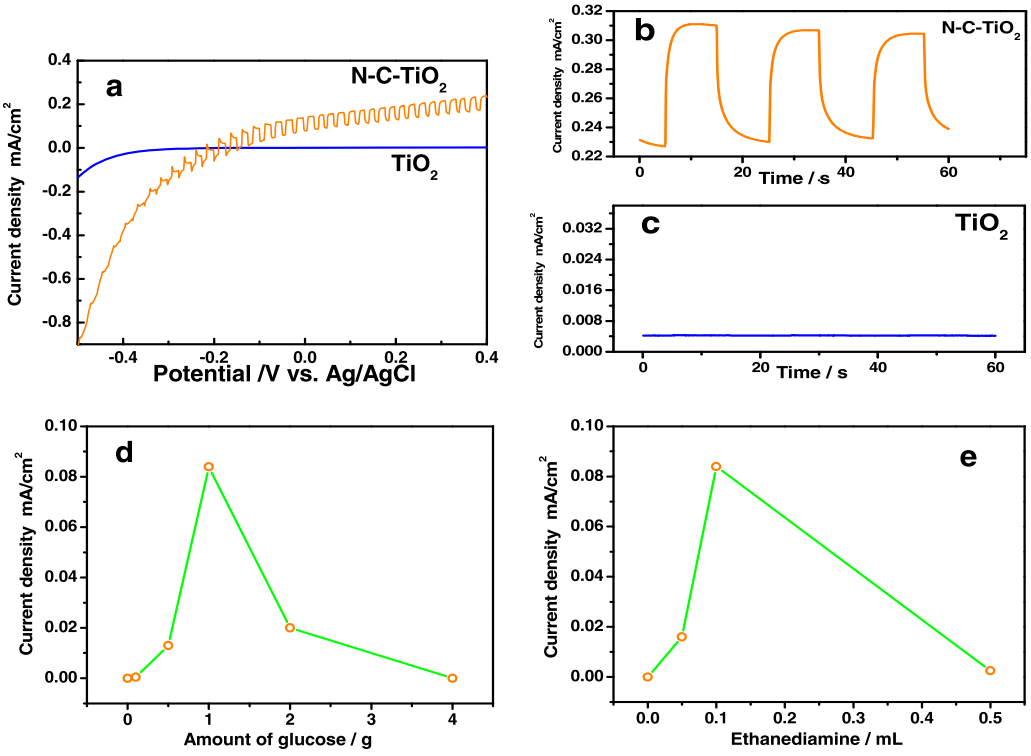

Fig. 3. (a) Linear sweep voltammogram collected from TiO_2 NRs (blue) and N—C—TiO_2 NRs (orange) under chopped radiation of a 2 W cm^{-2} 980 nm near infrared light laser. Transient photocurrent density measurements of (b) N—C—TiO_2 NRs and (c) TiO_2 NRs at 1.0 V vs. RHE in 0.1 M Na_2SO_4 solution. (d) Photocurrent density of N—C—TiO_2 NRs as a function of the amount of glucose used in the hydrothermal reaction at a fixed amount of ethanediamine 0.1 mL. (e) Photocurrent density of N—C—TiO_2 NRs as a function of the amount of ethanediamine used in the hydrothermal reaction at a fixed amount of glucose 1.0 mg. (For interpretation of the references to color in this figure legend, the reader is referred to the web version of this article.)

With a bandgap of 3.2 eV, the TiO_2 NRs cannot be excited by the near infrared photon. As a result, the photoresponse under near infrared irradiation is negligible, but it becomes observable with the N—C layer coated (Fig. 3b and c). With an on-set potential of −0.3 V vs. Ag/AgCl, the photocurrent reaches about 0.084 mA cm^{-2} at 0.4 V vs. Ag/AgCl, as can be seen in Fig. 3a. Probably, the N-doped carbon layer produces electrons and holes by harvesting the near infrared photons, and generates photocurrent accordingly.

Furthermore, the N-doped carbon layer was optimized to reach maximum NIR-driven activity by adjusting the amount of glucose and ethanediamine. As shown in Fig. 3d and e, with increasing amount of glucose and ethanediamine, the photocurrent rises and reaches the climax at 1.0 g glucose and 0.1 mL ethanediamine, but it diminished with excess glucose and ethanediamine.

Besides near infrared light, the N—C—TiO_2 NRs is photoactive under UV and visible light. As shown in Fig. 4a, the photocurrents of the photoanode increase gradually with increasing potential. Under AM 1.5 G simulated sunlight, the photucurrent reaches a saturated current of 0.55 mA cm^{-2} without any filter, 0.35 mA cm^{-2} with a 420 nm UV cut-off filter and 0.06 mA cm^{-2} with a 800 nm UV–vis cut off filter. This suggests that the N—C—TiO_2 NRs system is a wide-spectrum-sensitive photoanode.

The photocurrent of bare TiO_2 NRs is presented as a reference (dash line in Fig. 4a). With increasing bias, the photocurrent of N—C—TiO_2 NRs rises much faster than that of bare TiO_2 NRs due to the contribution from the N—C layer. Meanwhile, a negative shift of about 0.1 V is observed. Such a shift is mainly due to the additional photovoltage (V_{ph}) generation from the N—C layer [25]. As shown in Fig. S4, the V_{ph} of N—C—TiO_2 NRs (0.155 V) is larger than that of the bare TiO_2 NRs (0.098 V). These suggests than the N—C layer is advantageous to the TiO_2 NRs photoanode.

3.3. Efficiency of the photoanodes

The applied bias photon-to-current efficiency (ABPE) of water splitting on the N—C—TiO_2 photoanode was evaluated based on the equation bellows (Fig. 4c) [3]:

$$\eta = j_p \times (1.23 - |E_{RHE}|)/I_0 \quad (1)$$

where η is the efficiency of PEC water splitting, j_p the photocurrent density at the measured potential, I_0 the power density of incident light (100 mW cm^{-2}), and E_{RHE} the bias potential vs. RHE.

The measured potential vs. Ag/AgCl reference electrode ($E_{Ag/AgCl}$) were converted to the reversible hydrogen electrode (RHE) scale according to the Nernst equation [3,5]:

$$E_{RHE} = E_{Ag/AgCl} + 0.059pH + E^0_{Ag/AgCl} \quad (2)$$

where E_{RHE} is the converted potential vs. RHE, $E_{Ag/AgCl}$ the measured potential against Ag/AgCl reference electrode, and $E^0{}_{Ag/AgCl}$ the standard potential of Ag/AgCl at 25 °C.Under simulated sunlight illumination (100 mW cm^{-2}), the efficiency as a function of applied potential exhibits a volcano curve with a summit at 0.76 V vs. RHE. With a <420 nm UV cut off filter (80 mW cm^{-2}), the curve seems to be congruent with that without the filter. The ABPE efficiency of N—C—TiO_2 under Vis light illumination is identical with that under UV light. This demonstrates that the coating of the N—C layer on TiO_2 NRs extends its utilization of sunlight from the UV region to the Vis region with the same ABPE efficiency. This is of great significance because the Vis light account for a majority of energy in the sunlight spectrum. Moreover, the N—C—TiO_2 NRs also show photoresponse under NIR although its ABPE efficiency is about one-third of that under full spectrum illumination.

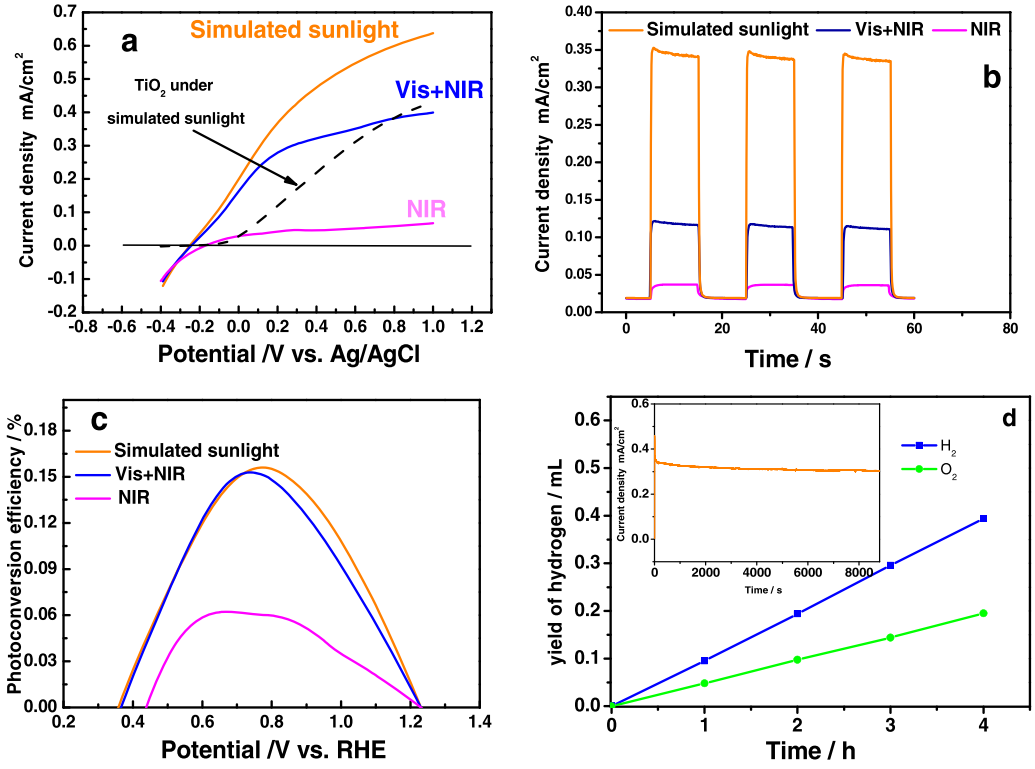

Fig. 4. (a) Under simulated solar illumination (AM 1.5G, 100 mW cm^{-2}), Linear sweeps voltammogram collected from N—C—TiO_2 NRs without any filter (orange), with a 420 nm UV cut-off filter (blue) and with a 800 nm UV–vis cut-off filter (magenta); The dash line correspond to the photocurrent of bare TiO_2 NRs under simulated sunlight (b) Transient photocurrent density measurements of N—C—TiO_2 NRs at 1.0 V vs. RHE in 0.1 M Na_2SO_4 solution; (c) Applied bias photon-to-current efficiency (ABPE) of water splitting on the N—C—TiO_2 NRs under different light sources; (d) Hydrogen and oxygen evolution from N—C—TiO_2 NRs at 1.0 V vs. RHE under simulated solar illumination (AM 1.5 G, 100 mW cm^{-2}), insert is the time course of photocurrent generation. (For interpretation of the references to color in this figure legend, the reader is referred to the web version of this article.)

The solar to gas efficiency can be determined by monitoring the yield of hydrogen and oxygen at 1.0 V vs. RHE. Since this potential is lower than the theoretical potential for water splitting by electrolysis, all the gases are formed by photocatalysis. Under illumination, hydrogen bubbles can be observed from the Pt cathode, as shown in Fig. S6. The yield of hydrogen is 0.110 mL/h, while that of oxygen is 0.054 mL/h. The 2:1 ratio of H_2 vs. O_2 confirms the water splitting reaction. The photocurrent was also monitored, as shown in the inset of Fig. 4d. The steady photocurrent and steady hydrogen evolution indicate that the N—C—TiO_2 NRs has high stability. The Faradaic efficiencies for hydrogen evolution and oxygen evolution are found to be 87.7% and 86.1%, respectively. This suggests the photocurrent is mainly due to water splitting. The stability of the N—C layer was confirmed by the integrity of the N—C layer after photoelectrochemical reaction (see the TEM images in Fig. S7a–b). As shown in Fig. S7c, we observed no color change in the samples after reaction. The photocurrent was maintained at 90% of its initial maximum value (insert in Fig. 4d), and the oxygen evolution exhibited good linearity (Fig. 4d). All these observations suggest that the N—C layer is stable during the photoelectrochemical process.

3.4. Mechanism

Based on the observation above, the N—C layer is of great significance for the utilization of Vis and NIR light. Its structure is studied by solid-state ^{13}C CP-MAS NMR (Fig. 5b), the peaks between 14 and 60 ppm, at 175 ppm and at 200 ppm correspond to aliphatic carbon, carboxyl carbon, and ketones, respectively. Importantly, the high and broad peaks between 100 and 160 ppm indicate the presence of numerous sp^2-hybridized structures in the N—C layer [26–28]. This

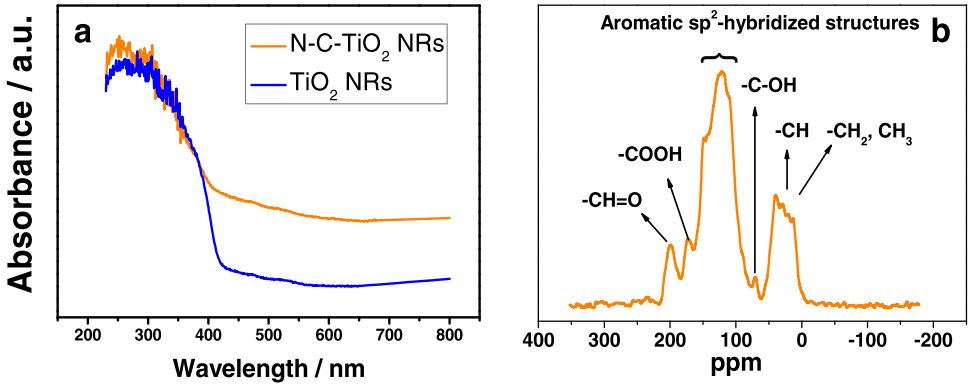

Fig. 5. (a) UV–vis diffuse reflectance spectra of TiO_2 NRs, N—C—TiO_2. (b) 13 C Solid-state NMR of the N—C materials.

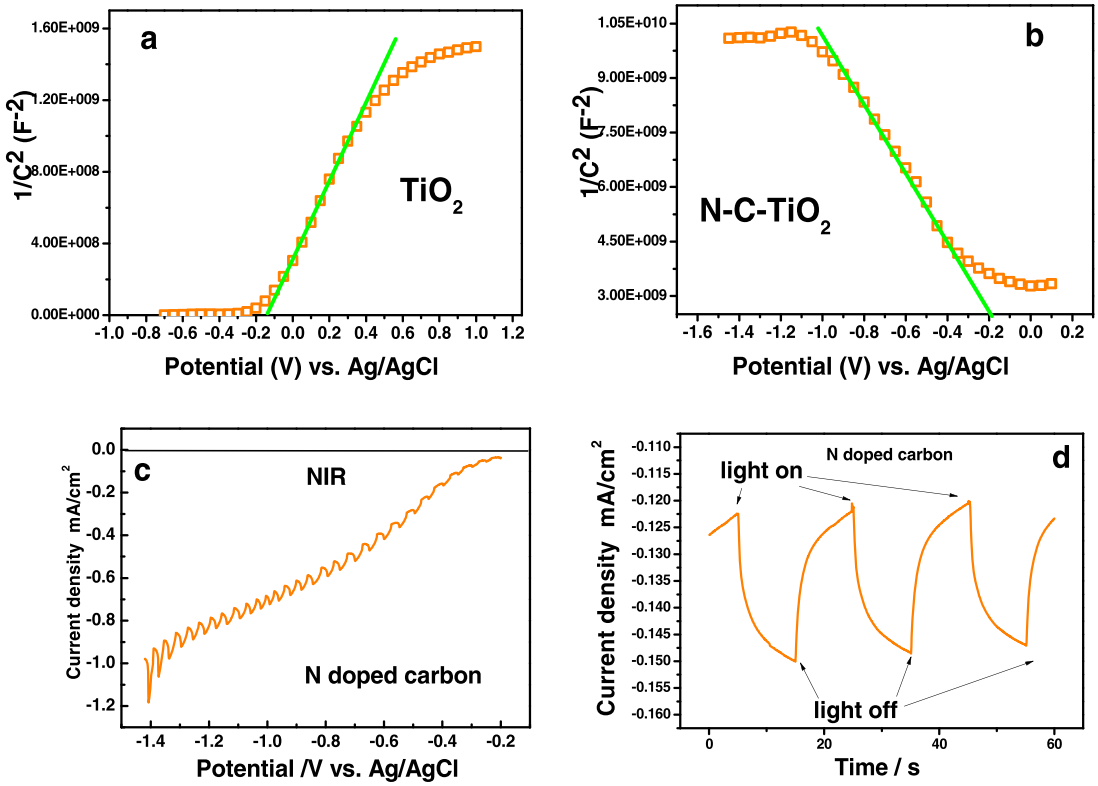

Fig. 6. Mott–Schottky plots of (a) TiO_2 NRs and (b) N—C—TiO_2 NRs at a frequency of 1000 Hz in 0.1 M Na_2SO_4 solution; (c) Cathodic scan of N—C—TiO_2 NRs in in 0.1 M Na_2SO_4 solution with a scan rate of 5 mVs−1; (d) Transient photocurrent measurement at −0.45 V vs. Ag/AgCl under near infrared light.

is due to the aromatization of glucose molecules under hydrothermal condition.

Those sp^2-hybridized structures are crucial for the N—C—TiO_2 photoanode because they can absorb visible and NIR light to generate free photoexcited electrons or holes. As shown in the UV–vis diffuse reflectance spectra, TiO_2 NRs absorbs only UV light, while the N—C—TiO_2 NRs exhibits a broad absorption from 300 to 900 nm (Fig. 5a).

The generation of photoexcited carriers from the N—C layer can be confirmed by the photocurrent measurement. In our experiment, a layer of N—C was deposited on a bare FTO without TiO_2 NRs covered. Cathodic photocurrent is produced and raised with increasing cathodic bias under chopped illumination of NIR (Fig. 6c). Meanwhile, repeatable cathodic photocurrent is produced noticeably in the transient photocurrent measurement under −0.45 V vs. Ag/AgCl (Fig. 6d). As discussed before, holes severs as majority carrier in p-type semiconductor, while electrons in n-type semiconductors. Under cathodic bias, cathodic current can only be formed via the flow of holes to the external circuit from p-type semiconductor (Scheme S1) [29,30].

The p-type property of the N—C layer can also be proved in the Mott–Schottky plots qualified by the following equation [31–33]:

$$\frac{1}{C^2} = \frac{2}{\epsilon \times \epsilon_0 \times e_0 \times N_D}\left(E - E_{FB} - \frac{kT}{e_0}\right) \quad (3)$$

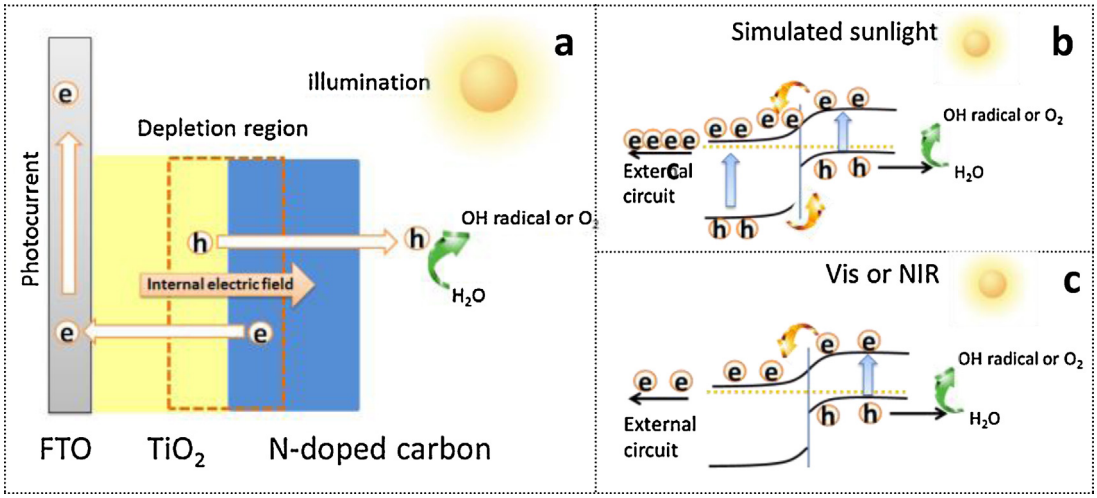

Scheme 2. (a) Schematic diagram showing the flow of charges in a *p–n* junction of N-doped carbon/TiO_2 NRs; Energy band of N—C—TiO_2 NRs under (b) simulated sunlight and (c) Vis or NIR illumination.

where C is the space charge capacitance, ϵ and ϵ_0 are the permittivity of the electrode and free space, e_0 the elementary charge, E the applied potential, E_{FB} the flatband potential, k the Boltzmann's constant, and T the temperature.

According to literatures, the slope in the Mott–Schotty plots mainly depends on surface capacitance. A positive slope for TiO_2 NRs characterizes a typical n-type semiconductor surface (Fig. 6a) [17]. By contrast, a negative slope for the N—C—TiO_2 NRs indicates that the coating of the N—C layer transfers the surface from n-type into p-type (Fig. 6b). This suggests that the N—C layer may behave like a p-type semiconductor.

Based on the discussion above, a tentative mechanism is proposed. A *p–n* junction was formed between the p-type N—C layer and the n-type TiO_2 NRs on the photoanode. According to the literature, an internal electric field is established between them via the diffusion of electrons from the n-type TiO_2 to the p-type N—C, and the holes in a contrary direction [34]. At anodic bias, the external and internal electric field is identical in direction. The photogenerated carriers can be transferred more efficiently with the aid of an anodic bias.

Under simulated sunlight illumination, photogenerated carriers are produced in both TiO_2 and the N—C layer. The internal electric field draws the photogenerated holes to the surface of N—C for water oxidation, and directs the photogenerated electrons to the external circuit for photocurrent generation (Scheme 2b). Even though TiO_2 is not visible-light active, photogenerated carriers can still be produced in the N—C layer under Vis or NIR irradiation. Therefore, photocurrent will be generated even under visible-light or NIR illumination (Scheme 2c).

4. Conclusions

A nitrogen-doped carbonaceous layer was decorated uniformly and intimately on the surface of TiO_2 nanorod array. The layer extends the utilization of solar energy of the TiO_2 nanorod array from UV to NIR region. The IPCE of N—C—TiO_2 NRs maintains at about 0.5–2.0% in the Vis region (420–800 nm), and about 0.1–0.5% in the NIR region (>800 nm). The high activity can be explained by the *p–n* junction established between the p-type nitrogen-doped carbonaceous layer and the n-type TiO_2.

Acknowledgements

The work described in this paper was partially supported by the Shenzhen Basic Research Scheme (JCYJ20120619151417947) and a grant from the Research Grants Council of the Hong Kong Special Administrative Region, China, under Theme-based Research Scheme through Project No. T23-407/13-N.

Appendix A. Supplementary data

Supplementary data associated with this article can be found, in the online version, at http://dx.doi.org/10.1016/j.apcatb.2015.01.018.

References

[1] Z.S. Li, W.J. Luo, M.L. Zhang, J.Y. Feng, Z.G. Zou, Energy Environ. Sci. 6 (2013) 347–370.
[2] S.R. Pendlebury, M. Barroso, A.J. Cowan, K. Sivula, J.W. Tang, M. Gratzel, D. Klug, J.R. Durrant, Chem. Commun. 47 (2011) 716–718.
[3] M. Xu, P.M. Da, H.Y. Wu, D.Y. Zhao, G.F. Zheng, Nano Lett. 12 (2012) 1503–1508.
[4] S. Sakthivel, M. Janczarek, H. Kisch, J. Phys. Chem. B 108 (2004) 19384–19387.
[5] S. Hoang, S.W. Guo, N.T. Hahn, A.J. Bard, C.B. Mullins, Nano Lett. 12 (2012) 26–32.
[6] Z.H. Xu, J.G. Yu, Nanoscale 3 (2011) 3138–3144.
[7] Z.H. Zhang, L.B. Zhang, M.N. Hedhili, H.N. Zhang, P. Wang, Nano Lett. 13 (2013) 14–20.
[8] Q.C. Xu, D.V. Wellia, Y.H. Ng, R. Amal, T.T.Y. Tan, J. Phys. Chem. C 115 (2011) 7419–7428.
[9] L.T. Su, S.K. Karuturi, J.S. Luo, L.J. Liu, X.F. Liu, J. Guo, T.C. Sum, R.R. Deng, H.J. Fan, X.G. Liu, A.I.Y. Tok, Adv. Mater. 25 (2013) 1603–1607.
[10] X. Zhang, H. Huang, J. Liu, Y. Liu, Z.H. Kang, J. Mater. Chem. A 1 (2013) 11529–11533.
[11] R. Trevisan, P. Rodenas, V. Gonzalez-Pedro, C. Sima, R.S. Sanchez, E.M. Barea, I. Mora-Sero, F. Fabregat-Santiago, S. Gimenez, J. Phys. Chem. Lett. 4 (2013) 141–146.
[12] D. Hulicova-Jurcakova, A.M. Puziy, O.I. Poddubnaya, F. Suarez-Garcia, J.M.D. Tascon, G.Q. Lu, J. Am. Chem. Soc. 131 (2009) 5026.
[13] T. Maiyalagan, A.A. Nassr, T.O. Alaje, M. Bron, K. Scott, J. Power Sources 211 (2012) 147–153.
[14] N. Lebedev, S.A. Trammell, S. Tsoi, A. Spano, J.H. Kim, J. Xu, M.E. Twigg, J.M. Schnur, Langmuir 24 (2008) 8871–8876.
[15] L.J. Yang, S. Wang, Q.S. Zeng, Z.Y. Zhang, L.M. Peng, Small 9 (2013) 1225–1236.
[16] Q. Liu, B.D. Guo, Z.Y. Rao, B.H. Zhang, J.R. Gong, Nano Lett. 13 (2013) 2436–2441.
[17] G.M. Wang, H.Y. Wang, Y.C. Ling, Y.C. Tang, X.Y. Yang, R.C. Fitzmorris, C.C. Wang, J.Z. Zhang, Y. Li, Nano Lett. 11 (2011) 3026–3033.
[18] M. Sevilla, A.B. Fuertes, Carbon 47 (2009) 2281–2289.
[19] X.M. Sun, Y.D. Li, Angew. Chem. Int. Ed. 43 (2004) 597–601.
[20] H.S. Qian, S.H. Yu, L.B. Luo, J.Y. Gong, L.F. Fei, X.M. Liu, Chem. Mat. 18 (2006) 2102–2108.
[21] M.S. Lazarus, T.K. Sham, Chem. Phys. Lett. 92 (1982) 670–673.
[22] E. McCafferty, J.P. Wightman, Surf. Interface Anal. 26 (1998) 549–564.
[23] F.-X. Ma, J. Wang, F.-b Wang, X.H. Xia, Chem. Commun. 51 (2015) 1198–1201.
[24] X.B. Chen, L. Liu, P.Y. Yu, S.S. Mao, Science 331 (2011) 746–750.
[25] C. Du, X.G. Yang, M.T. Mayer, H. Hoyt, J. Xie, G. McMahon, G. Bischoping, D.W. Wang, Angew. Chem. Int. Ed. 52 (2013) 12692–12695.
[26] R. Demir-Cakan, N. Baccile, M. Antonietti, M.M. Titirici, Chem. Mater. 21 (2009) 484–490.
[27] J.Z. Hu, M.S. Solum, C.M.V. Taylor, R.J. Pugmire, D.M. Grant, Energy Fuels 15 (2001) 14–22.
[28] Z.R. Shen, G.J. Zhang, H.J. Zhou, P.C. Sun, B.H. Li, D.T. Ding, T.H. Chen, Adv. Mater. 20 (2008) 984.
[29] J.N. Nian, C.C. Tsai, P.C. Lin, H.S. Teng, J. Electrochem. Soc. 156 (2009) H567–H573.
[30] L.B. Xiong, S. Huang, X. Yang, M.Q. Qiu, Z.H. Chen, Y. Yu, Electrochim. Acta 56 (2011) 2735–2739.
[31] X.Y. Yang, A. Wolcott, G.M. Wang, A. Sobo, R.C. Fitzmorris, F. Qian, J.Z. Zhang, Y. Li, Nano Lett. 9 (2009) 2331–2336.
[32] C. Baumanis, D.W. Bahnemann, J. Phys. Chem. C 112 (2008) 19097–19101.
[33] T.V. Nguyen, O.B. Yang, Catal. Today 87 (2003) 69–75.
[34] J.T. Li, F.K. Meng, S. Suri, W.Q. Ding, F.Q. Huang, N.Q. Wu, Chem. Commun. 48 (2012) 8213–8215.